Articles

Novel Photo-Cross-Linkable Hole-Transporting Polymers: Synthesis, Characterization, and Application in Organic Light Emitting Diodes

Steffen Jungermann,[†] Nina Riegel,[‡] David Müller,[‡] Klaus Meerholz,*[,‡] and Oskar Nuyken*[,†]

Lehrstuhl für Makromolekulare Stoffe, Technische Universität München, Lichtenbergstrasse 4, 85747 Garching, Germany, and Institut für Physikalische Chemie, Universität zu Köln, Luxemburgerstrasse 116, 50939 Köln, Germany

Received April 14, 2006; Revised Manuscript Received October 6, 2006

ABSTRACT: Novel polymeric hole-transporters **P1** through **P4** were synthesized based on triarylamine units in the backbone with pendant oxetane groups which can be used for photo-cross-linking. These polymers were characterized by NMR spectroscopy, GPC, IR spectroscopy, and DSC. Their electrochemical properties were investigated by means of cyclic voltammetry. Multilayer organic light emitting devices were fabricated layer by layer using inexpensive solution based methods like spin-coating followed by a cross-linking step. UV spectroscopy was used to prove that the spin-coated layers are totally insoluble after the cross-linking process. The hole-transport capabilities of the polymers were evaluated in hole-only devices and finally multilayer OLEDs were fabricated to test the performance of the synthesized compounds.

1. Introduction

The first polymeric light emitting diodes were single-layer devices with an emitting layer between two electrodes.[1,2] In those devices high charge-injection barriers, low mobility of charge-carriers (holes and electrons) and a recombination zone close to the cathode led to rather low efficiencies and lifetimes. Better characteristics have been achieved by changing the device structure to a multilayer design with designated layers for electron and hole-transport, made of special customized materials. In the class of hole-transport materials, compounds based on triarylamines exhibit outstanding hole-transporting capabilities.[3] Polymeric OLED materials allow for the use of inexpensive solution casting methods like spin-coating for layer fabrication, taking advantage of their very good film-forming properties and high film stability. However, the solution based preparation of multilayer OLEDs introduces the problem that already coated layers tend to be at least partially dissolved by the solvent used to apply the next layer. A common method used to overcome this obstacle is to render the applied layer insoluble by cross-linking before the next coating step.[4−9] In our approach, we use the oxetane functionality attached to triarylamine based hole-transport polymers as a photopolymerizable moiety.[9−11] The choice of the oxetane group is based on the fact, that like other cyclic ethers, it can undergo fast cationic polymerization in bulk with high conversion and low volume shrinkage, avoiding cracks in the spin-coated layers.[12,13] During device processing, a solution of the polymer mixed with small amounts of a photosensitive cationic initiator is spin-coated on the substrate and cross-linked by UV irradiation, which leaves the resulting insoluble film ready for the application of the next layer. An additional advantage of the oxetane group is its characteristic IR band, which allows for realtime observation of the progress of the photopolymerization with a special FT-IR setup.

If the goal is to build high performance OLED displays for use in, e.g., mobile applications the different layers have to be structured to form pixels and subpixels. Such patterning processes include the use of inkjet printing[14,15] or screen printing[16] with solutions of polymeric OLED materials. They have many advantages, but compared to spin-coated devices, these methods still show some major drawbacks like inhomogeneous wetting of the surface which makes prestructuring of the substrate necessary. Another approach to high resolution patterning is based on photolithography by cross-linking of, e.g., oxetane functionalities initiated by UV irradiation. By usage of shadow masks in the process of illumination, the material not only becomes insoluble but also can simultaneously be patterned like a negative photoresist.[17−20]

In the past we have established several strategies to build cross-linkable hole-transport materials with incorporated oxetane functionalities:[9] Low-molecular-weight charge-transport molecules,[10] nonconjugated polymers with charge-transporters as a part of the polymer backbone,[21] and side-chain-functionalized polymers with an inert poly(styrene) backbone and pendant charge-transporters.[22] The cross-linkable oxetane groups are located in the side chains in all these cases. In this paper we present a novel class of main-chain polymeric hole-transport materials based on triarylamines. The oxetane moiety is connected to the triarylamine-backbone via flexible hexyl spacers to guarantee high diffusional mobility. In the following chapters

* Corresponding authors. (O.N.) Telephone: +498928913571. Fax: +498928913562. E-mail: oskar.nuyken@mytum.de. (K.M.) Telephone: +492214703275. Fax: +492214705144. E-mail: klaus.meerholz@uni-koeln.de.

[†] Lehrstuhl für Makromolekulare Stoffe, Technische Universität München.

[‡] Institut für Physikalische Chemie, Universität zu Köln.

10.1021/ma060844o CCC: $33.50
Published on Web 11/24/2006

the synthesis of these materials is described. They are thoroughly characterized regarding their chemical and physical properties, cross-linking qualities (realtime FT-IR-measurements and solubility tests), hole-transport capabilities (hole-only devices), and qualification for the application in OLEDs (multilayer test devices).

2. Experimental Section

2.1. Materials. All reagents were purchased from Aldrich, Lancester or Merck and were used without further purification. All solvents were dried using standard laboratory procedures. The syntheses were carried out under nitrogen or argon atmosphere using standard Schlenk or glovebox techniques. For better handling purposes, the purified polymers were freeze-dried from benzene solution. Given concentrations of the photoinitiator $\mathbf{I}^+$ are always based on the oxetane content of the polymers, i.e., at the same molar concentration (for example 1 mol %) the absolute amount of initiator added to a 100% oxetane functionalized polymer (**P1**, **P2**, **P3**) is twice the absolute amount added to a 50% oxetane functionalized polymer (**P4**).

2.2. Instrumentation. ^{1}H NMR (300 MHz) and ^{13}C NMR (75 MHz) spectra were obtained on a Bruker ARX 300 spectrometer and were calibrated relative to the solvent peak in reference to tetramethylsilane standard. Peaks are listed in parts per million (ppm) downfield from tetramethylsilane. Gel permeation chromatography (GPC) was performed on a system consisting of a Waters pump 510 and a refractive index detector (model 410) with PLG Mixed C columns. Samples were dissolved in chloroform and filtered through a 0.22 μm Teflon membrane (Millipore) before injection. Molecular weights were calibrated with polystyrene standards. UV/vis experiments were carried out on a Varian Cary 3 spectrophotometer. Elemental analysis was performed by the microanalytical laboratory of the "Anorganisch-chemisches Institut", TU München. FT-IR spectra (ATR and films on silicon wafers) were recorded on a Bruker IFS 55 spectrometer. Differential scanning calorimetry (DSC) measurements were performed on a Mettler Toledo calorimeter model 821^e, calibrated by the melting point of indium. MALDI−TOF mass spectrometry was carried out on a Bruker Biflex III with dithranol as matrix and chloroform as solvent. A model 283 potentiostate/galvanostate from EG&G Instruments was applied for cyclic voltammetry (CV) studies.

2.3. Monomer and Polymer Synthesis. 3-(6-Bromohexyloxymethyl)-3-ethyloxetane (1). 3-Ethyl-3-hydroxymethyloxetane (11.62 g, 0.1 mol) and 1,6-dibromohexane (73.19 g, 0.3 mol) in 400 mL of *n*-hexane and 100 g of 45 wt % aqueous NaOH were refluxed for 6 h in the presence of tetrabutylammonium bromide (1.61 g, 5.0 mmol). Then the reaction mixture was cooled to room temperature, and 200 mL of water was added. This mixture was extracted with *n*-hexane, and the combined organic phases were dried over $MgSO_4$. After removal of the solvent, the residue was distilled in vacuo, resulting in a colorless liquid (14.67 g, 53%).

$C_{12}H_{23}BrO_2$ (279.21 g·mol^{-1}), bp: 100 °C (4 mbar). ^{1}H NMR ($CDCl_3$): δ = 4.42, 4.35 (d, 2 × 2H, $^2J_{H-H}$ = 5.7 Hz, $(CH_2)_{oxetane}$); 3.50 (s, 2H, $-O-CH_2-(C)_{oxetane}$); 3.40 (m, 2 × 2H, $BrCH_2-C_4H_8-CH_2O-$); 1.85 (m, 2H, $BrCH_2CH_2-$); 1.72 (q, 2H, $^3J_{H-H}$ = 7.4 Hz, $-CH_2CH_3$); 1.58 (m, 2H, $-CH_2CH_2O-$); 1.39 (m, 4H, $-CH_2-$); 0.86 (t, 3H, $^3J_{H-H}$ = 7.4 Hz, $-CH_3$). ^{13}C NMR ($CDCl_3$): δ = 78.39 ($(CH_2)_{oxetane}$); 73.31 ($-O-CH_2-(C)_{oxetane}$); 71.19 ($-CH_2-CH_2O-$); 43.28 ($(C)_{oxetane}$); 33.66 ($BrCH_2CH_2-$); 32.59 ($BrCH_2-$); 29.22; 27.81; 26.64 ($-CH_2-CH_2-CH_2-CH_2O-$); 25.23 ($-CH_2-CH_3$); 8.07 ($-CH_3$). Anal. Calcd: C, 51.62; H, 8.30. Found: C, 51.90; H 8.30.

3-[6-(4-Bromophenoxy)hexyloxymethyl]-3-ethyloxetane (2). 4-Bromophenole (8.65 g, 0.05 mol) and potassium carbonate (13.82 g, 0.10 mol) were dissolved in 200 mL of DMSO, and **1** (12.56 g, 0.045 mol) was added. This mixture was stirred for 4 h at 65 °C, cooled to room temperature, and then diluted with 200 mL of water and extracted with diethyl ether three times. The combined organic layers were dried with $MgSO_4$, and the solvent was evaporated. The residue was fractionated by flash chromatography on silica with cyclohexane/ethyl acetate (4:1 v/v) yielding a light yellow liquid (16.28 g, 97%).

$C_{18}H_{27}BrO_3$ (371.31 g·mol^{-1}). ^{1}H NMR ($CDCl_3$): δ = 7.33 (d, 2H, $^3J_{H-H}$ = 9.0 Hz, H^2_{Ar}, H^6_{Ar}); 6.74 (d, 2H, $^3J_{H-H}$ = 9.0 Hz, H^3_{Ar}, H^5_{Ar}), 4.43, 4.35 (d, 2·2H, $^2J_{H-H}$ = 5.7 Hz, $(CH_2)_{oxetane}$); 3.89 (t, 2H, $^3J_{H-H}$ = 6.4 Hz, $-OCH_2CH_2-$); 3.50 (s, 2H, $-OCH_2-(C)_{oxetane}$); 3.44 (t, 2H, $^3J_{H-H}$ = 6.3 Hz, $-CH_2O-$); 1.73 (m, 2·2H, $-OCH_2CH_2-$, $-CH_2CH_3$); 1.59 (m, 2H, $-CH_2CH_2O-$); 1.43 (m, 4H, $-CH_2-$); 0.86 (t, 3H, $^3J_{H-H}$ = 7.4 Hz, $-CH_3$). ^{13}C NMR ($CDCl_3$): δ = 158.14 (C^4_{Ar}); 132.10 (C^2_{Ar}, C^6_{Ar}); 116.21 (C^3_{Ar}, C^5_{Ar}); 112.51 (C^1_{Ar}); 78.51 ($(CH_2)_{oxetane}$); 73.35 ($-O-CH_2-(C)_{oxetane}$); 71.37 ($-CH_2CH_2O-$); 68.04 ($-OCH_2CH_2-$); 43.35 ($(C)_{oxetane}$); 29.29; 29.06; 26.71; 25.87 ($-OCH_2-C_4H_8-CH_2O-$); 25.77 ($-CH_2CH_3$); 8.13 ($-CH_3$). Anal. Calcd: C, 58.22; H, 7.33. Found: C, 57.81; H, 7.27.

***N,N′*-Di{4-[6-(3-ethyloxetane-3-methoxy)]hexyloxyphenyl}-benzidine (3).** A catalyst consisting of tris(dibenzylideneacetone)-dipalladium(0) (Pd_2dba_3) (0.274 g, 0.3 mmol) and diphenylphosphinoferrocene (0.499 g, 0.9 mmol) dissolved in 30 mL toluene and preformed by stirring for 10 min at room temperature was added to benzidine (2.76 g, 15.0 mmol), **2** (11.14 g, 30.0 mmol), and sodium-*tert*-butylate (4.33 g, 45.0 mmol) dissolved in 120 mL toluene. This mixture was stirred for 4 h at 95 °C and then cooled to room temperature, diluted with water, and extracted with diethyl ether. The ether phase was dried with $MgSO_4$, and the solvent was evaporated. The residue was fractionated by repeated column chromatography on silica gel with cyclohexane/ethyl acetate (1:1 v/v) yielding a white solid (3.71 g, 32%).

$C_{48}H_{64}N_2O_6$ (765.03 g·mol^{-1}). MALDI−TOF: m/z = 764.9; 765.9; 766.9; 767.9 g·mol^{-1}, which matches the simulated pattern of $(C_{48}H_{64}N_2O_6)^+$. ^{1}H NMR (CD_2Cl_2): δ = 7.42 (d, 4H, $^3J_{H-H}$ = 8.8 Hz, H^2_{Ar}); 7.08 (d, 4H, $^3J_{H-H}$ = 8.8 Hz, H^3_{Ar}); 6.96 (d, 4H, $^3J_{H-H}$ = 8.6 Hz, H^7_{Ar}); 6.86 (d, 4H, $^3J_{H-H}$ = 8.6 Hz, H^6_{Ar}); 5.63 (s, 2H, −N*H*); 4.40, 4.31 (d, 2·4H, $^2J_{H-H}$ = 5.7 Hz, $(CH_2)_{oxetane}$); 3.94 (t, 4H, $^3J_{H-H}$ = 6.5 Hz, $-OCH_2CH_2-$); 3.51 (s, 4H, $-OCH_2-(C)_{oxetane}$); 3.47 (t, 4H, $^3J_{H-H}$ = 6.5 Hz, $-CH_2O-$); 1.74 (m, 2·4H, $-OCH_2CH_2-$, $-CH_2CH_3$); 1.62 (m, 4H, $-CH_2CH_2O-$); 1.47 (m, 2·4H, $-CH_2-$); 0.88 (t, 6H, $^3J_{H-H}$ = 7.4 Hz, $-CH_3$).

^{13}C NMR ($CDCl_3$): δ = 155.16; 144.26; 136.08; 132.56; 127.37; 122.12; 116.27; 115.67 (C_{Ar}); 78.58 ($(CH_2)_{oxetane}$); 73.76 ($-O-CH_2-(C)_{oxetane}$); 71.79 ($-CH_2CH_2O-$); 68.72 ($-OCH_2CH_2-$); 43.76 ($(C)_{oxetane}$); 29.93; 29.73; 27.27; 26.37; 26.27 ($-OCH_2-C_4H_8-CH_2O-$, $-CH_2CH_3$); 8.33 ($-CH_3$). Anal. Calcd: C, 75.36; H, 8.43; N, 3.66. Found: C, 75.06; H, 8.44; N, 3.53.

General Procedure for C—N-Coupling Polymerization GP1. Tris(dibenzylideneacetone)dipalladium(0) (Pd_2dba_3) (18.3 mg, 0.02 mmol) and tris(*tert*-butyl)phosphine (8.1 mg, 0.04 mmol) were dissolved in 2 mL of toluene under argon and stirred for 10 min at room temperature. This activated catalyst was then added to a mixture of **3** (0.765 g, 1.0 mmol), sodium-*tert*-butylate (0.269 g, 2.8 mmol), and 1.0 mmol of a dibromoarylic monomer (**4**, **5**, or **6**) in 18 mL of toluene. The reaction mixture was stirred for 18 h at 100 °C, and then 10 mL of toluene was added. For end-capping purposes, first diphenylamine (6.76 mg, 0.04 mmol) and 1 h later bromobenzene (9.42 mg, 0.06 mmol) were added. After another hour, the mixture was cooled to 75 °C and 8 mL of aquaous diethyldithiocarbamate solution (5% w/w) were added. The reaction mixture was stirred vigorously for 2 h and then diluted with water and centrifuged twice to separate the organic layer from the aqueous phase. The polymer was then precipitated by dropping the organic phase into a 10-fold excess of methanol. The precipitated polymer was filtered, redissolved in chlorobenzene and precipitated again in an excess of methanol. Finally the polymer was freeze-dried from benzene.

General Procedure for C—N-Coupling Copolymerization GP2. In the case of hole-transport copolymer **P4** with reduced oxetane content, the activated catalyst as in **GP1** was added to a mixture of **3** (0.383 g, 0.5 mmol), *N,N′*-diphenylbenzidine (**3′**) (0.168 g, 0.5 mmol), sodium-*tert*-butylate (0.269 g, 2.8 mmol), and 4,4′-dibromobiphenyl (**4**) (0.312 g, 1.0 mmol) in 18 mL of toluene.

Scheme 1. Synthesis of Monomer 3

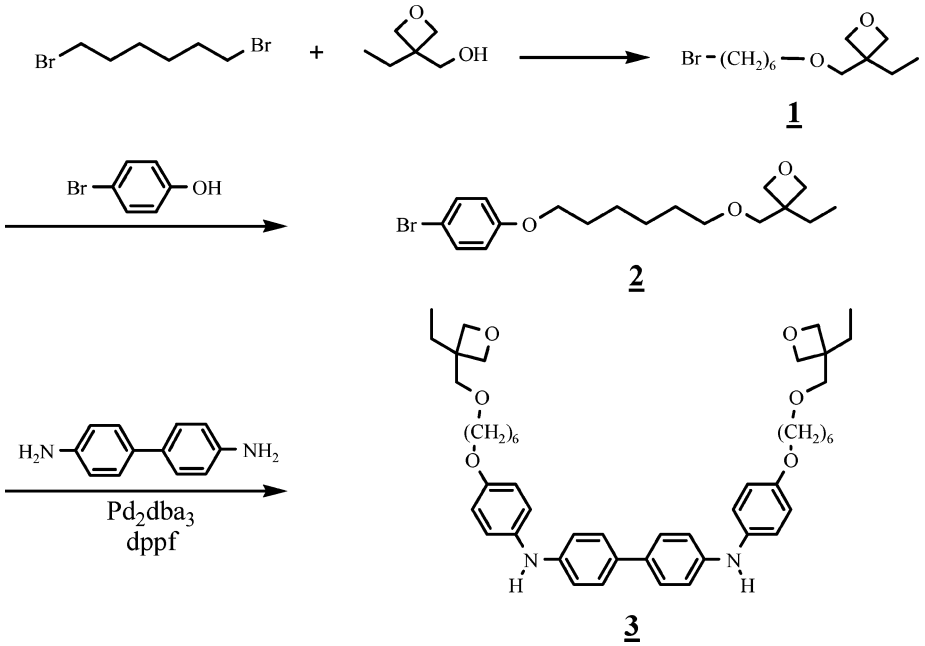

The reaction and purification procedure was the same as described above.

Polybiphenylene—OxTPD (P1). P1 was synthesized according to the general polymerization procedure **GP1**. 4,4′-Dibromobiphenyl (**4**) (0.312 g, 1.0 mmol) was used as second monomer. The product was obtained as a light yellow powder (0.813 g, 88%).

$(C_{60}H_{70}N_2O_6)_n$ (915.21 g·mol^{-1})$_n$. ^{1}H NMR (CD_2Cl_2): δ = 7.50−6.80 (m, 24H, H_{Ar}); 4.41, 4.32 (d, 2·4H, (CH_2)$_{oxetane}$); 3.96 (t, 4H, −OCH_2CH$_2$−); 3.52 (s, 4H, −OCH_2−(C)$_{oxetane}$); 3.48 (t, 4H, −CH_2O−); 1.80−1.40 (m, 20 H, (−OCH$_2$−C_4H_8−CH$_2$O−, −CH_2-CH$_3$); 0.88 (t, 6H, −CH_3). IR (film from THF): ν = 3027, 2929, 2856, 1598, 1486, 1373, 1315, 1272, 1234, 1178, 1162, 1105, 1022, 977, 817, 721, 638 cm^{-1}. GPC ($CHCl_3$, RI): M_n = 17 640 g·mol^{-1}; M_w = 40 790 g·mol^{-1}; PDI = 2.31.

Poly-*p*-phenylene—OxTPD (P2). P2 was synthesized according to the general polymerization procedure **GP1.** 1,4-Dibromobenzene (**5**) (0.236 g, 1.0 mmol) was used as the second monomer. The product was obtained as a light yellow powder. (0.755 g, 90%).

$(C_{54}H_{66}N_2O_6)_n$ (839.11 g·mol^{-1})$_n$. ^{1}H NMR (CD_2Cl_2): δ = 7.45−6.80 (m, 20H, H_{Ar}); 4.40, 4.31 (d, 2·4H, (CH_2)$_{oxetane}$); 3.95 (t, 4H, −OCH_2CH$_2$−); 3.51 (s, 4H, −OCH_2−(C)$_{oxetane}$); 3.47 (t, 4H, −CH_2O−); 1.75−1.40 (m, 20 H, (−OCH$_2$−C_4H_8−CH$_2$O−, −CH_2-CH$_3$); 0.87 (t, 6H, −CH_3). IR (film from THF): ν = 3030, 2931, 2860, 1603, 1496, 1373, 1311, 1269, 1238, 1165, 1107, 1024, 980, 822, 717 cm^{-1}. GPC ($CHCl_3$, RI): M_n = 9990 g·mol^{-1}; M_w = 17 160 g·mol^{-1}; PDI = 1.72.

Polyfluorenylene—OxTPD (P3). P3 was synthesized according to the general polymerization procedure **GP1**. 1,4-Dibromofluorenyl (**6**) (0.324 g, 1.0 mmol) was used as the second monomer. The product was obtained as a light yellow powder (0.707 g, 76%).

$(C_{61}H_{70}N_2O_6)_n$ (927.22 g·mol^{-1})$_n$. ^{1}H NMR (CD_2Cl_2): δ = 7.55−6.80 (m, 22H, H_{Ar}); 4.40, 4.31 (d, 2·4H, (CH_2)$_{oxetane}$); 3.95 (t, 4H, −OCH_2CH$_2$−); 3.72 (s, 4H, (CH_2)$_{fluorene}$); 3.51 (s, 4H, −OCH_2−(C)$_{oxetane}$); 3.47 (t, 4H, −CH_2O−); 1.80−1.40 (m, 20 H, (−OCH$_2$−C_4H_8−CH$_2$O−, −CH_2CH$_3$); 0.86 (t, 6H, −CH_3). IR (film from THF): ν = 3027, 2929, 2861, 2730, 1725, 1604, 1504, 1492, 1467, 1363, 1295, 1270, 1238, 1176, 1106, 1022, 980, 817, 696 cm^{-1}. GPC ($CHCl_3$, RI): M_n = 8300 g·mol^{-1}; M_w = 12 230 g·mol^{-1}; PDI = 1.47.

Poly(biphenylene—TPD—biphenylene—OxTPD) (P4). P4 was synthesized according to the general polymerization procedure **GP2.** 1,4-Dibromobiphenyl (**4**) (0.312 g, 1.0 mmol) was used as the second monomer. The product was obtained as a light yellow powder (0.602 g, 86%).

$(C_{96}H_{96}N_4O_6)_n$ (1401.81 g·mol^{-1})$_n$. ^{1}H NMR (CD_2Cl_2): δ = 7.43−6.85 (m, 50H, H_{Ar}); 4.39, 4.31 (d, 2·4H, (CH_2)$_{oxetane}$); 3.94 (t, 4H, −OCH_2CH$_2$−); 3.50 (s, 4H, −OCH_2−(C)$_{oxetane}$); 3.47 (t, 4H, −CH_2O−); 1.76−1.46 (m, 20 H, (−OCH$_2$−C_4H_8−CH$_2$O−, −CH_2CH$_3$); 0.87 (t, 6H, −CH_3). IR (film from THF): ν = 3027, 2929, 2856, 1598, 1486, 1369, 1315, 1272, 1234, 1178, 1164, 1106, 1022, 978, 817, 721, 694 cm^{-1}. GPC ($CHCl_3$, RI): M_n = 10 410 g·mol^{-1}; M_w = 37 170 g·mol^{-1}; PDI = 3.57.

2.4 Realtime ATR−IR Measurements. The hole-transport polymers **P1**−**P4** (50 mg·mL^{-1}) and a variable amount of photoinitiator $\mathbf{I}^+$ (Scheme 4) were dissolved in dry THF or dry dichloromethane (1−5 mol % based on the oxetane content). By placing a droplet (or droplets) of the solution directly on the heated ATR crystal (80 °C) and letting it dry, thin polymer films were obtained. Under these conditions thermal initiation of the reaction can be neglected. The sample was then irradiated with UV light from a waveguided Hg UV lamp-beam while IR spectra are periodically measured. The whole experiment took place in a flowbox-like inert gas atmosphere. The oxetane peak at 980 cm^{-1} was integrated to calculate the oxetane conversion. To eliminate environmental errors of the setup and achieve best possible comparability, all measurements are normalized on the 5 mol % series of polymer **P1** at 80 °C. In these series no oxetane signal can be observed after 180 s of illumination so that quantitative oxetane conversion can be assumed. Each time fresh solutions were prepared, and a new normalization run was measured.

2.5. Solubility Tests. Commercially available microscope slides were used as substrates for the solubility tests. They were cut to the size of 2.5 × 2.5 cm^2 and cleaned by ultrasonic treatment in chloroform, acetone and an alkaline cleaning solution (Mucasol). The following steps were carried out under red light illumination which does not activate the photoinitiator and therefore premature cross-linking can be avoided. The polymers **P1**−**P4** were dissolved in dry toluene (10 mg·mL^{-1}) and mixed with varying amounts of the photoinitiator $\mathbf{I}^+$ (0.5−5 mol %, based on the oxetane content; $\mathbf{I}^+$ is dissolved in THF) directly before spincoating. Layers of around 50 nm thickness were formed from 300 μL of these solutions, which were spin-coated on the glass substrates inside of a glovebox. The films were then cross-linked with UV light for one second (λ = 365 nm) and cured at 100 or 150 °C to enhance chain mobility. The degree of insolubility of the films was investigated by comparison of UV spectra before and after washing with THF which is an excellent solvent for the non-cross-linked polymers. Simply rinsing with THF showed to be equally capable

Scheme 2. Synthesis of Homopolymers P1, P2 and P3—General Procedure GP1

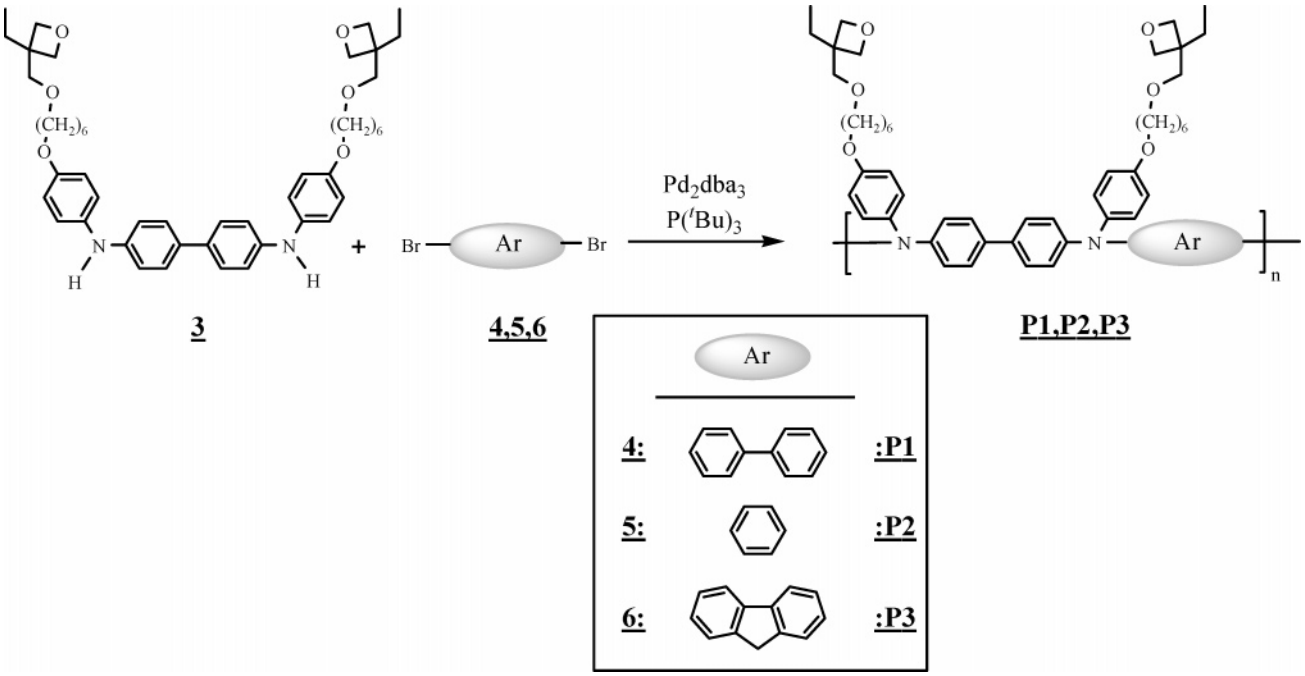

Scheme 3. Synthesis of Copolymer P4—General Procedure GP2

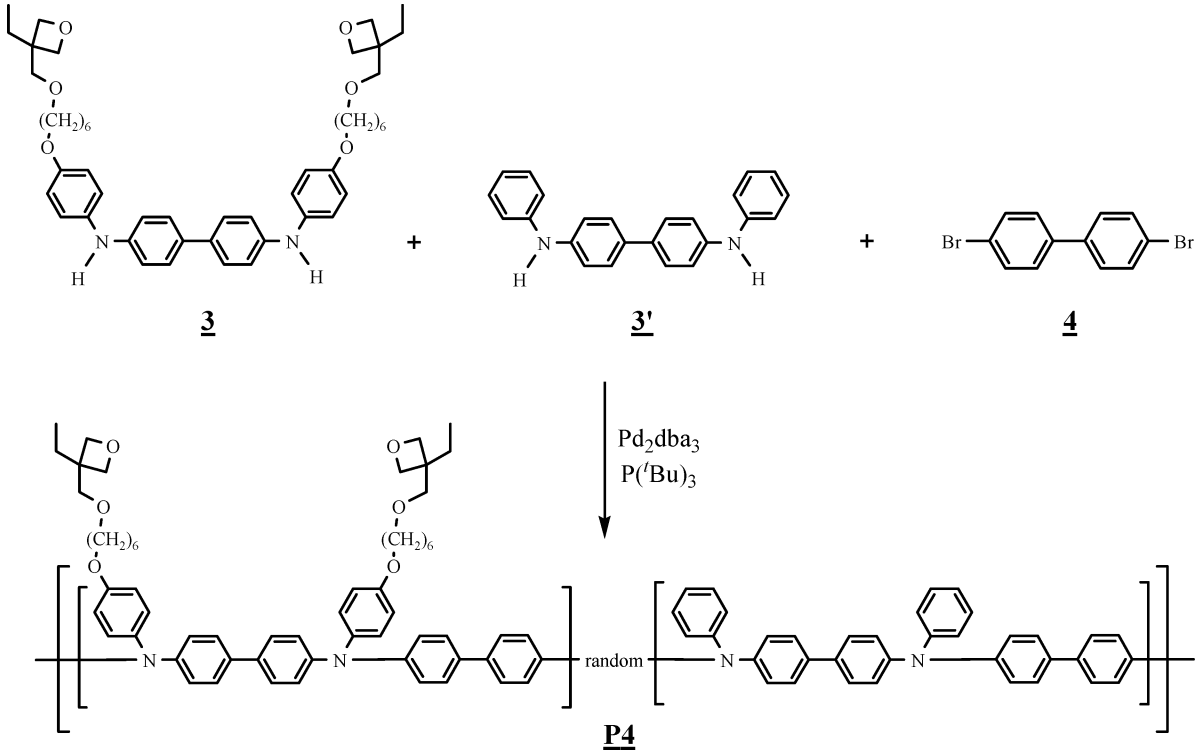

of removing all non-cross-linked polymers as immersing the films in THF for a few minutes with ultrasound.

2.6. Device Preparation. Hole-only devices (HOD) and organic light-emitting devices (OLED) are based on ITO (indium tin oxide) coated glass substrates, which are commercially available from Merck (20 $\Omega\cdot$in.$^{-2}$). These were cut and cleaned analogous to the glass substrates used for the solubility tests (see section 2.5 above). After drying the ITO surface was treated in an ozone plasma to raise its hydrophilicity. Then 35 nm of poly(3,4-ethylenedioxythiophen) (PEDOT; Baytron P AL4083, HC Stark) were spin-coated on top of the ITO as hole-injecting contact.

For hole-only devices, a solution of 25 mg$\cdot$mL^{-1} of **P1**−**P4** in toluene containing various amounts of photoinitiator $\mathbf{I}^+$ (0−3 wt %, based on the oxetane content; $\mathbf{I}^+$ is dissolved in THF) was spin-coated on the PEDOT layer to yield a single layer of about 100 nm thickness. Cross-linking was achieved by short UV-illumination (λ = 365 nm, 1 s) and a tempering step at 150 °C for 1 min. Afterward, the layer was rinsed with THF to remove all soluble remains and byproducts of the photoinitiation. Finally, the silver cathode (150 nm) was vapor deposited on top of the device.

OLEDs were fabricated by spin-coating as three-layer-devices on top of the PEDOT surface following the film deposition procedure as outlined above. First a layer of the polymers **P1**−**P4** of 20 nm thickness was applied and cross-linked with 3% $\mathbf{I}^+$ (curing at 100 °C) followed by a 10 nm layer of monomeric hole-transport material **TPD1** (see Scheme 4; cross-linked with 0.5 mol % $\mathbf{I}^+$,

Scheme 4. Chemical Structures of the Iodonium Photoinitiator I^+ and the Low-Molecular-Weight Hole-Transport Materials TPD1 and TPD2 Used as References[a]

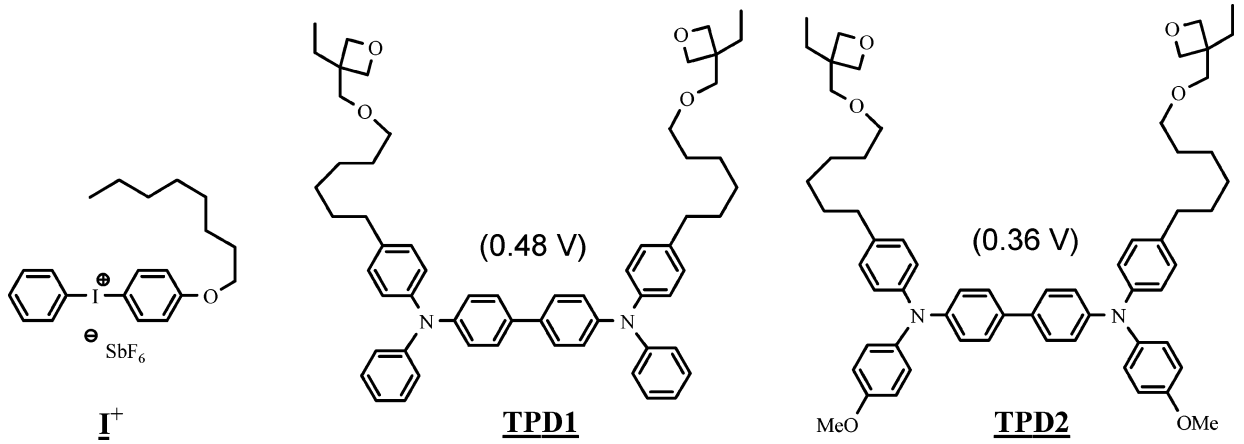

I⁺ **TPD1** **TPD2**

[a] The oxidation potentials E_{Ox} of the monomeric hole-transport materials Are given in parentheses.

curing at 150 °C). A state-of-the-art blue emitting polymer on spirofluorene basis (Covion Organic Semiconductors) was spin-coated on top of the hole-transport materials from toluene solution (10 mg·mL^{-1}) to yield a thickness of 80 nm. On top of the device, the cathode consisting of 5 nm barium followed by 150 nm silver was vacuum deposited.

The characterization of the HODs and OLEDs was performed by a custom-made voltage generator using a calibrated ampere meter and a calibrated photodiode. All steps up to the PEDOT deposition were performed in air under clean room conditions, and all further layer deposition steps and device characterization were performed in a glovebox under inert gas atmosphere. Consecutive runs show a deviation of less than 10%.

3. Results and Discussion

3.1. Synthesis. The polymers **P1**−**P4** with the triarylamine functionality in the backbone were prepared via a polycondensation reaction of the A_2B_2-type. This synthetic strategy has the advantage that one complex A_2-monomer (in this case bearing the oxetane functionalities) can be polymerized with a variety of more simple B_2-monomers to give a kind of molecular "construction kit". A drawback of this approach (polycondensation in general) is the relatively high demands in terms of monomer purity. Since the type of the backbone connection has an influence on the electrochemical properties, it is thus possible to form polymers which are customized in their redox properties to match the requirements of the desired multilayer OLED device (electrode work functions and HOMO levels of the next layer).

Monomer Synthesis. The oxetane functionalized A_2-monomer **3** is obtained in a three-step synthesis (see Scheme 1) starting from commercially available educts 1,6-dibromohexane and 3-ethyl-3-hydroxymethyloxetane. The hexyl spacer is attached to the oxetane functionality via basic etherification to give 3-(6-bromohexyloxymethyl)-3-ethyloxetane (**1**). The bromo end group is then replaced by 4-bromophenole to give 3-[6-(4-bromophenoxy)hexyloxymethyl]-3-ethyloxetane (**2**). Two equivalents of **2** were coupled via Hartwig-Buchwald amination[23,24] with benzidine. The reaction is suited for the aimed purpose because the reactivity of primary amines is higher than the reactivity of secondary amines. Therefore, the symmetric coupling of 1 equiv of **2** at each amine group yielding the monomer *N*,*N*′-di{4-[6-(3-ethyloxetane-3-methoxy)]-hexyloxyphenyl}benzidine (**3**) as the main product is favored over a multiple coupling. This tendency is amplified by the use of diphenylphosphinoferrocene as relatively inactive ligand. Nonetheless, a mixture of all four chemically rather similar reaction products is obtained, and the desired product has to be isolated via several purification steps.

Table 1. Polymer Characterization and Cross-Linking Rates/Final Oxetane Conversion of the Cross-Linking of Polymers P1−P4 (See Section 3.2) at 50 °C with 3% of Photoinitiator I^+ (Molar Based on the Oxetane Content)

	P1	P2	P3	P4
yield[a] [%]	88	90	76	86
M_n [b]	17 640	9990	8300	10 410
M_w [b]	40 790	17 160	12 230	37 170
PDI[b]	2.31	1.72	1.47	3.57
ratio **3**:**3**′ [c]				1:1.07
E_{ox} [V] vs ferrocene[d]	0.43	0.18	0.32	0.52
$\lambda_{max,abs}$ [nm]	384	374	400	376
T_g [°C]	96	58	73	137

Cross-Linking at 50 °C with 3% I^+

P1		P2		P3		P4	
b_{50}	convn [%]	b_{50}	convn [%]	b_{50}	convn [%]	b_{50}	convn [%]
80	69	249	49	16	14	41	18

[a] Isolated yield. [b] Determined by GPC with polystyrene standards. [c] Determined by ^{1}H NMR. [d] Average value of anodic and cathodic peak potentials.

Polymer Synthesis and Characterization. For polymerization purposes the Hartwig-Buchwald amination is utilized as A_2B_2-polycondensation reaction[25] with a diamine monomer (**3**, **3**′) and various dibromo aromatic compounds (**4**, **5**, **6**) Since there are only secondary amine functionalities in the A_2-monomers there is no need for reaction control and a very active catalyst system with tris(*tert*-butyl)phosphine as ligand is used to achieve high conversion.[26]

Polymers **P1**, **P2**, and **P3** were synthesized from A_2-diamine monomer **3** and B_2-monomers dibromobiphenyl (**4**), 1,4-dibromobenzene (**5**), and dibromofluorenyl (**6**) in strict 1:1 ratios (see Scheme 2). To get a polymer with reduced oxetane content, copolymer **P4** was synthesized by copolycondensation of **3**, the oxetane-free analogue *N*,*N*′-diphenylbenzidine **3**′, and B_2-compound **4** in a 1:1:2 ratio (see Scheme 3). The resulting copolymer is similar to **P1** with the difference that it is only 50% oxetane functionalized, to test the influence of the number of oxetanes in the polymer chains on the photo-cross-linking process.

Molecular weights were measured by gel permeation chromatography (GPC) in chloroform relative to poly(styrene) standards (see Table 1). All polymers were received in moderate to good yields with number-avaraged molecular weights between

8000 and 17000 g·mol^{-1} and PDI values between 1.7 and 3.6. The ratio of oxetane-functionalized and oxetane-free repeating units in copolymer **P4** can be approximated from the ^{1}H NMR spectra by comparison of the aromatic protons and the oxetane protons. A ratio of 1:1.07 was found, which is nearly the monomer feed ratio of 1:1; i.e., every second repeating unit contains two oxetane functionalities. In this approximation, the end-capping units are not included.

Differential scanning calorimetry (DSC) was used to measure the glass transition temperatures (T_g) of the non-cross-linked polymers. This value is important for device preparation purposes because the temperature of the curing step after UV illumination should be chosen higher than the T_g of the polymer to raise the diffusional mobility of the oxetane groups in the film to ensure complete cross-linking. Polymers **P1**−**P3** showed T_g's below 100 °C while **P4** has a T_g of 137 °C (see Table 1). Therefore, a curing temperature of 100 °C should be sufficient for the cross-linking of layers of **P1**, **P2**, and **P3**, but could be too low to guarantee a completely insoluble layer of cross-linked **P4**.

UV−vis absorption spectra were recorded to evaluate the optical properties of the hole-transport polymers. The polymers **P1**, **P2**, and **P4** possess absorption maxima between 374 and 384 nm, **P3** shows a maximum at 400 nm which we contribute to the incorporated fluorene units.

The electrochemical properties of the cross-linked polymers (3 mol % of photoinitiator $\mathbf{I}^+$) were investigated by cyclic voltammetry (CV) with spin-coated films of 100 nm thickness on ITO-coated glass substrates. The solvent was acetonitrile and tetrabutylammonium hexafluorophosphate 0.1 mol/L was added as conductive salt. All polymers showed reversible oxidation and therefore qualify for the application in OLEDs. The oxidation potentials relative to ferrocene, which was used as internal standard, are given in Table 1. They range from 0.18 to 0.52 V which allows for an electronic grading of hole-transport multilayers ("electronic stairs") to facilitate hole injection and to choose the best suited hole-transport compound for a given emitter material.

3.2. Realtime ATR—IR Measurements. Solutions of hole-transport polymers **P1**−**P4** were mixed with variable amounts of a photoinitiator (iodonium salt $\mathbf{I}^+$; Scheme 4) and cross-linked by irradiation with UV light.

Upon exposure to UV irradiation the photoacid decomposes in multiple steps and generates protons which start the cationic ring-opening polymerization of the oxetane moieties. The oxetane ring shows a characteristic IR band at 980 cm^{-1} (asymmetric stretch vibration). The conversion of the oxetanes can be followed in realtime by registration of this characteric absorption using a specially developed ATR setup (*a*ttenuated *t*otal *r*eflection). Parameters that influence the cross-linking process include temperature, initiator concentration, polymer backbone, and oxetane content of the polymer. During illumination the intensity of the oxetane band at 980 cm^{-1} is decreasing while simultanously certain signals in the area between 1175 and 1020 cm^{-1} are increasing due to the formation of linear polyethers. To compare the kinetic measurements we used an estimation for the cross-linking rate with the time τ_{50} needed to reach 50% of the final oxetane conversion level and the corresponding rate $b_{50} = 1/\tau_{50}$.

The final level of oxetane conversion in the hole-transport polymers increases with the concentrations of $\mathbf{I}^+$. For example, in polymer **P1** the values rise from 35% (1 mol % $\mathbf{I}^+$) to 76% (2 mol %) and finally to quantitative conversion (5 mol % $\mathbf{I}^+$), the 5 mol % series being more than twice as fast as the 2 mol % series and around five times as fast as the 1 mol % series. This can be explained by the fact that more oxetanes are initiated throughout the film by a higher number of initiator molecules. These active starting points are then able to reach and open more oxetane groups and the polymerization rate is high and limited only by the diffusion of the active chain ends through the forming network. Increasing viscosity during cross-linking and thus reduced mobility is a reason for incomplete conversion of the oxetane units at lower initiator concentrations. A cross-linking temperature of 80 °C in the experiments, i.e., below the glass transition temperature, is chosen intentionally to slow the photopolymerization down and accentuate the differences between the single measurements. At normal curing temperatures of 100 or even 150 °C, the cross-linking process would be too fast to give significant discrepancies in the IR spectra. At lower temperatures (30 and 50 °C were investigated with polymer **P1**) the cross-linking rates as well as the final oxetane conversion levels are significantly lower since the diffusional mobility through the forming network is limited in dependency of the temperature.

In comparison with similar low-molecular-weight compounds, which we studied earlier,[10,11] which have glass transition temperatures below room temperature, both, the rate of photopolymerization and the final oxetane conversion of the polymeric hole-transport materials are lower. At 80 °C and 1 mol % $\mathbf{I}^+$, the cross-linking of monomeric compounds is about 1 order of magnitude faster and reaches around 70% oxetane conversion compared to 36% for the polymeric material **P1**. This fact can be attributed to the lower diffusional mobility of oxetane groups attached to polymer chains (higher T_g).

The lower part of Table 1 shows a comparison of the cross-linking parameters of the synthesized polymers **P1**−**P4** with 3 mol % photoinitiator $\mathbf{I}^+$ at 50 °C. There are significant differences between the polymers: **P2** showed the highest rate b_{50} but reached only around 50% oxetane conversion while the symmetrical and fully oxetane functionalized polymer **P1** polymerized to 69% oxetane conversion with a medium rate. Compared to this, the cross-linking rate of 50% oxetane functionalized polymer **P4** is reduced by a factor of 2, and the cross-linking stops after 18% oxetane conversion. This could be due to the greater interspace between the oxetane groups. The photopolymerization of **P3** shows an overall lower performance under these conditions and also stops after just 14% oxetane conversion.

3.3. Solubility Tests. The realtime IR-measurements showed that the oxetane rings are consumed during UV illumination and cross-linking of the layer. They also showed a dependence of the final oxetane conversion on the amout of photoinitiator added, but they give no information on the practical aspect of solvent resistivity/insolubility of the layers in the OLED fabrication process. All synthesized polymers in their non-cross-linked state are readily soluble in common organic solvents like toluene, chloroform, and THF. After cross-linking, they should be completely insoluble. UV−vis spectroscopy was used to test the efficiency of the cross-linking process. Absorption intensities of cross-linked poly-TPD layers before and after rinsing the layer with THF were compared. According to the conditions during device production after the short UV illumination (usually just a second is enough) a curing step at up to 150 °C is carried out to soften the geling film and so to enhance the diffusional mobility of the active carbo-cation chain ends and to ensure complete cross-linking.

Figure 1 shows the results for the two similar polymers **P1** and **P4** which differ in the amount of oxetane groups in the

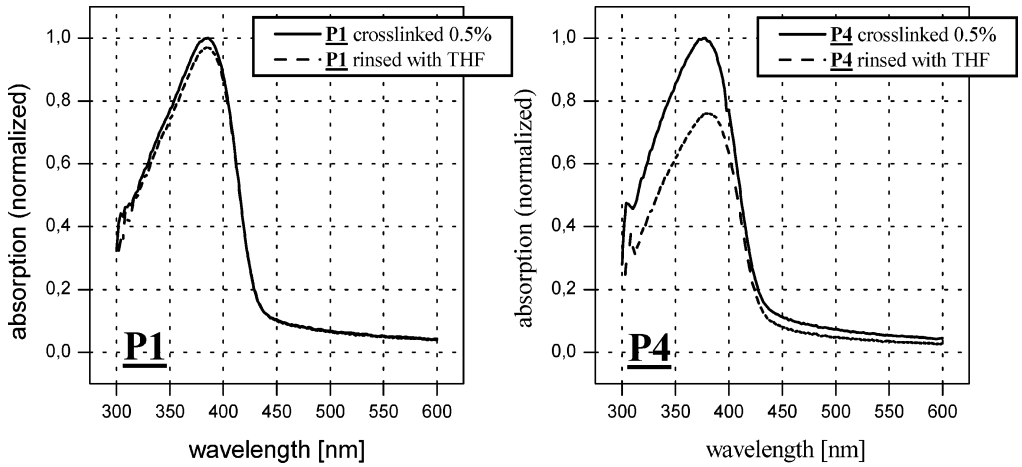

Figure 1. Solvent resistivity test by means of UV/vis spectroscopy of cross-linked layers of **P1** and **P4** with 0.5% of photoinitiator $\mathbf{I}^+$. Curing was performed for 1 min at 150 °C, and spectra were taken after cross-linking and after rinsing with THF.

Table 2. Influence of $\mathbf{I}^+$ Concentration (based on the oxetane content of the polymers) and Curing Temperature on the Solvent Resistivity of Cross-linked Layers of P1 and P4

	[$\mathbf{I}^+$] = 0.5 mol %		[$\mathbf{I}^+$] = 1 mol %		[$\mathbf{I}^+$] = 3 mol %		[$\mathbf{I}^+$] = 5 mol %	
	curing temp = 100 °C	curing temp = 150 °C	curing temp = 100 °C	curing temp = 150 °C	curing temp = 100 °C	curing temp = 150 °C	curing temp = 100 °C	curing temp = 150 °C
P1	96	97	100		100			
P4	69	76	94	96	98	99	100	100

polymer chains. Both layers are cross-linked with 0.5 mol % photoinitiator $\mathbf{I}^+$ (based on the oxetane content) and are cured at 150 °C for 1 min. While **P1** is almost insoluble in THF, the layer of **P4** exhibits only 76% solvent resistivity (SR). Analogous experiments of **P4** in the presence of higher concentrations of photoinitiator ($\mathbf{I}^+ \geq 1$ mol %) result in solvent resistivity up to 100%. The influence of the amount of photoinitiator added and the curing temperature on the solvent resistivity is compiled in Table 2.

The polymers **P2** and **P3** gave similar results, and complete solvent resistivity (within error range ≥96%) was achieved for all polymers with 3% of photoinitiator at a curing temperature of 100 °C with 1% of photoinitiator at a curing temperature of 150 °C, respectively.

If one compares the results from realtime IR kinetic measurements and the solubility tests at a given concentration of photoinitiator, it is remarkable that the layers of hole-transport polymers become insoluble although the oxetane conversion is far from being complete. In the case of polymer **P1**, total insolubility was achieved at 0.5% photoinitiator content even at room temperature. Under these conditions only around 4% oxetane conversion could be measured in IR experiments. This demonstrates the advantage of polymeric materials over low-molecular-weight compounds: not every cross-linkable unit has to react to render the layer insoluble. In theory, just two oxetane groups per chain should be sufficient to obtain a completely cross-linked network.

The direct comparison of **P1** and **P4** shows that 0.5 mol % of photoinitiator are sufficient to reach insolubility of **P1** while a layer of **P4** needs at least 1 mol %. Besides the lower number of oxetane functionalities in **P4**, this could also be an effect of the higher glass-transition temperature of **P4** (137 °C) compared to **P1** (96 °C). Attempts to get homogeneous polymers with lower oxetane content were either not successful or it was not possible to get insoluble layers up to now.

3.4. Hole-Transport Capabilities. The pristine hole-transport capabilities of the synthesized polymers were investigated in so-called hole-only devices. During the fabrication of these devices no photoinitiator was added to the layers. The silver cathode on top of the device creates a high injection barrier and therefore effectively inhibits the injection of electrons into the organic layer. In this way, only positive hole-charges are transported through the device. Figure 2 shows the current−voltage diagrams of hole-only devices consisting of non-cross-linked hole-transport polymers **P1**−**P4**. The polymers show onset voltages (defined here as voltage required for a current density of 0.1 mA/cm^2) between 3.4 and 5.0 V and are very stable, showing no degradation up to a current density of 1 A/cm^2. While the sequence of operating voltages is **P1** < **P3** < **P4** < **P2** for current below 100 mA/cm^2, this is **P1** < **P4** < **P3** < **P2** for current above 500 mA/cm^2; i.e., there is no clear trend. There are two factors determining the hole current in HODs, the hole injection barrier and the hole mobility. As the anode is identical in all cases, we expect the hole-injection barrier to increase in the sequence of the oxidation potentials (Table 1), i.e., **P2** < **P3** < **P1** < **P4.** Since the current performance does not follow this sequence, we conclude that the hole mobility in **P2** and **P3** is reduced compared to **P1** and **P4**.

The hole-transport characteristics of the synthesized polymers are greatly improved if the photoinitiator $\mathbf{I}^+$ is added and the layers are cross-linked as can be seen in Figure 2, which shows the current−voltage diagrams of polymers **P1** and **P4** with 1 and 2 mol % added photoinitiator $\mathbf{I}^+$ (based on the oxetane content). The onset voltages are reduced to 1.3 V for **P1** cross-linked with 2% initiator. The reason for this improvement is that the electron-rich, highly fluorescent triarlyamine compounds are efficient photosensitizers. Therefore, during UV illumination radical cations are formed in the hole-transport layer due to photoelectron transfer (PET) between the polymers and the initiator. These radical cations act as effective p-doping sites in the material and therefore facilitate hole transport. There is a direct correlation between the amount of doping and the oxidation potential of the polymer so that materials with lower oxidation potential form radical cations easier. This explains the order in the onset voltages at 0.1 mA/m^2 (**P1** < **P4**) with **P1** showing a lower oxidation potential than **P4**. **P2** and **P3** show results that are in agreement with this argumentation.

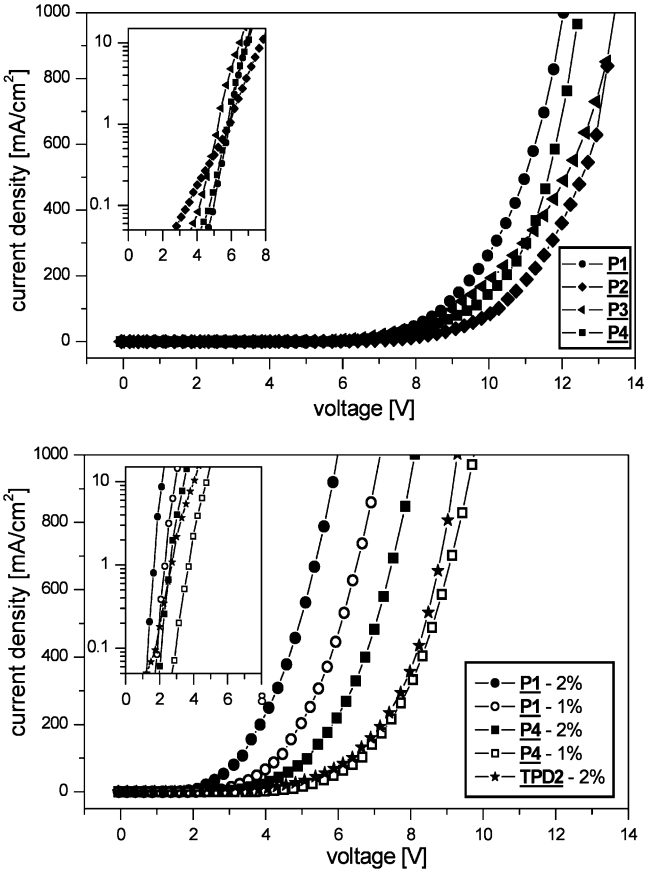

Figure 2. Current/voltage diagrams of hole-only devices of the general structure ITO/PEDOT/hole-transport layer (100 nm)/Ag (150 nm). Top: hole-transport layer consisting of non-cross-linked polymers **P1** through **P4**. Bottom: hole-transport layer consisting of cross-linked layers of hole-transport polymers **P1** and **P4** using 1 mol % (open symbols) or 2 mol % (filled symbols) of photoinitiator. For comparison, data for monomeric **TPD2** (Scheme 4) is shown for reference purposes (stars). The insets shows the same data in semilogarithmic scale.

Finally we point out that the hole current in a **TPD2**-based device cross-linked using 2 wt % of the initiator is similar to the current in a **P4**-device with 1wt % initiator, even though the oxidation potential is lower (0.36 in **TPD2** compared with 0.52 in **P4**). This clearly shows the superior hole-transprot performance of the fully conjugated main-chain polymer compared to the monomeric analogue.

3.5. Multilayer Organic Light Emitting Devices. The synthesized hole-transport polymers were tested in multilayer OLEDs. The positive effect of the radical cations, generated during the cross-linking process, on the hole-transport capabilities turns out to be a problem when these p-doped hole-transport layers are incorporated into OLEDs where they may quench the electroluminescence at the interface of HTL and emitting layer. To avoid this problem, the highly doped hole-transport material and the emitter material have to be separated by an additional nondoped hole-transport layer. For this purpose, we used the low-molecular-weight hole-transport material **TPD1** (see Scheme 4), to build a thin layer which was cross-linked with the least possible initiator amount (0.5 mol %) on top of the hole-transport polymer layer. The polymer layer was cross-linked with 3 mol % initiator to get a high doping level. As emitter material (**EL**) we used a non-cross-linkable blue one based on spirofluorenes[20] (Covion Organic Semiconductors, Frankurt).

Figure 3 shows the performance of these devices. Onset voltages to reach a current density of 0.1 mA/cm^2 were between

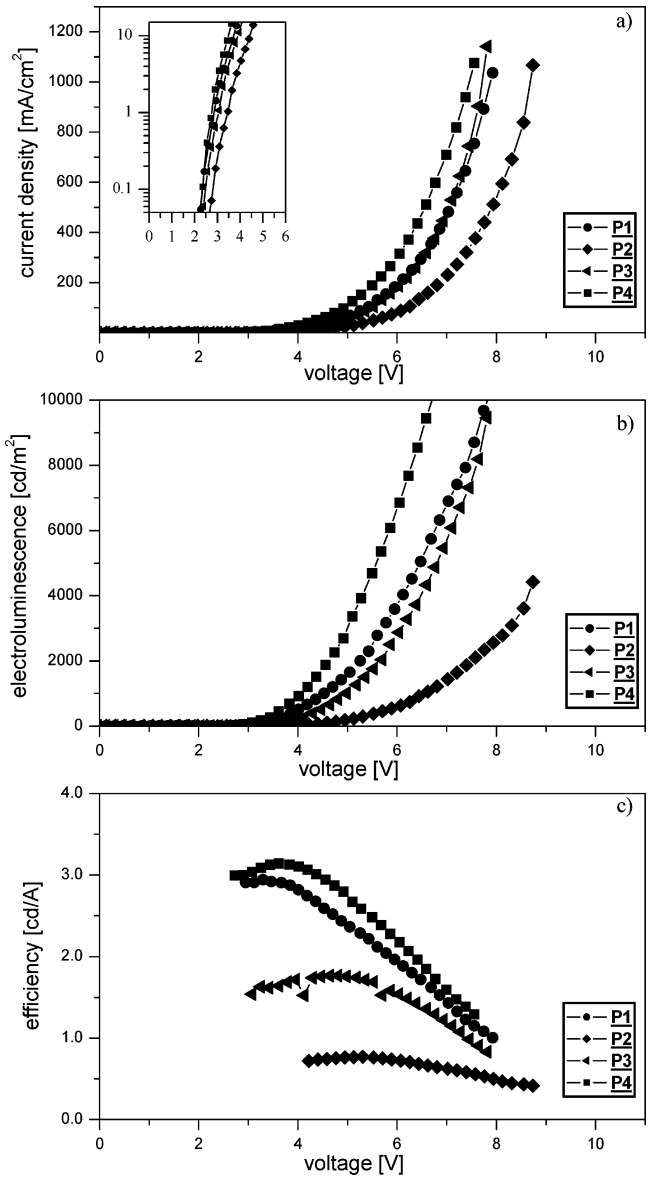

Figure 3. Performance data of cross-linked multilayer OLEDs of the general structure ITO/PEDOT/**P1** through **P4** (20 nm)/**TPD1** (10 nm)/**EL** (80 nm)/Ba (5 nm)/Ag (150 nm). Key:(a) current/voltage diagram (the inset shows the same data in semilogarithmic scale); (b) forward light output; (c) efficiency of the devices.

3.2 and 3.65 V, first light output (at 10 cd/m^2) was detected between 2.5 and 3.5 V and the electroluminescence reached maximum values of more than 13000 Cd/m^2 at about 8 V (**P4**). Maximum efficiencies range from very good 3.15 Cd/A in the case of **P4** to 0.78 Cd/A for **P2**. We attribute this to the fact that the electronic proportions inside the device (injection and transport barriers between the layers) are very dependent on the position of the HOMO level of the hole-transport material. The increase in maximum efficiency of multilayer OLEDs with polymer **P2** < **P3** <**P1** < **P4** in sequence with the rising oxidation potential is outlined in Figure 4. Accordingly the voltage required to reach a light output of 1000 cd/m^2 drops in reverse order. In the case of **P4** the oxidation potential seems to be optimally aligned to the other layers and leads to the very good characteristics.

For comparison, reference devices without additional hole-transport layer and identical thickness of the emitter (80 nm) exhibit an efficiency of about 1 Cd/A. The extrapolated half-brightness lifetime at an initial brightness of ~100 Cd/m^2 is in

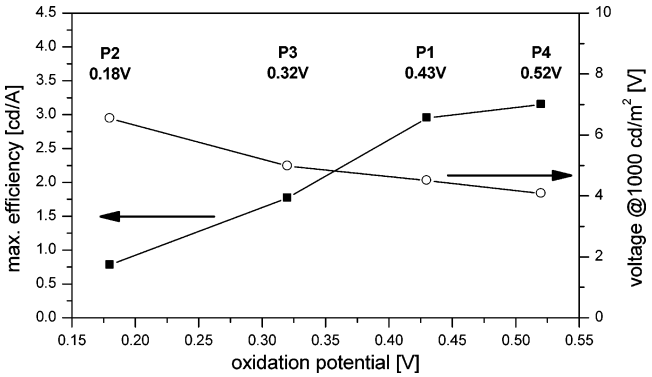

Figure 4. Maximum efficiency (filled squares) and voltage needed to reach a light output of 1000 Cd/m2 (open circles) plotted against the oxidation potential of the synthezised hole-transport polymers **P1** through **P4**.

Table 3. Emission Characteristics and Device Thicknesses (HTL and EL) of the Multilayer Test Devices

	P1	P2	P3	P4
λ_{max}	478	481	487	478
CIE *x*-value	0.17	0.19	0.18	0.17
CIE *y*-value	0.17	0.19	0.24	0.17
device thickness [nm]	117	110	119	111

the range of 100 h under continuous operation. During operation, all devices were color stable.

In Table 3, the maximum emission wavelength and the CIE values of the devices are depicted. While the emission properties of **P1** and **P4** are identical due to the similar composition of the OLED active functions, the emission of **P3** is shifted toward the greenish blue. This could be due to the specific optical properties of **P3** or is perhaps an effect of the incorporated fluorenyl units or oxidation of these fluorenes to fluorenones.

4. Conclusion

In conclusion, four novel polymeric hole-transport materials based on triarylamines with the charge- transporting functionality in the polymer backbone have been synthesized. These materials contain attached oxetane groups which are used to cross-link spin-coated layers by UV illumination. Realtime IR experiments have been carried out to obtain insights in the kinetics of the cross-linking process. Solubitity tests based on UV/vis spectroscopy have demonstrated the insolubility of the layers. These experiments will be used to further optimize the cross-linking parameters. Both, IR experiments and solubility tests, proved that the cross-linking approach via oxetane functionalities is fast and efficient and yields insoluble networks.

As cyclovoltammetric measurements showed a fully reversible oxidation of the triarylamin functionalities the synthesized hole-transport polymers were investigated regarding their charge-transport capabilities. All polymers showed good onset voltages between 3.5 and 5.0 V in the non-cross-linked state, which were lowered after cross-linking due to the formation of radical cations due to photoelectron transfer to the initiator. Multilayer organic light emitting diodes fabricated from some of these novel materials (**P4** and **P1**) and a blue emissive emitter exhibited excellent performance: a test OLED based on oxetane-poor **P4** showed a maximum efficiency of 3.15 Cd/A at less than 4 V. In the other cases (polymers **P2** and **P3**), the performance was reduced compared to the **P4**-based device due to unfavorable electric levels at the internal HTL/emitter interface.

Acknowledgment. Financial support provided by the Bundesministerium für Bildung und Forschung (BMBF) through Project 13N8214 and the Bavarian Government (Promotionsstipendium for S.J.) is gratefully acknowledged. We thank Dr. Ronald Alle for help with the electrochemical experiments and Dr. Markus Rojahn for the synthesis of the low-molecular-weight hole-transporters **TPD1** and **TPD2**.

References and Notes

(1) Tang, C. W.; VanSlyke, S. A. *Appl. Phys. Lett.* **1987**, *51*, 913.
(2) Burroughes, J. H.; Bradley, D. D. C.; Brown, A. R.; Marks, R. N.; Mackay, K.; Friend, R. H.; Burns, P. L.; Holmes, A. B. *Nature (London)* **1990**, *347*, 539.
(3) Thelakkat, M. *Macromol. Mater. Eng.* **2002**, *287*, 442.
(4) Li, W.; Wang, Q.; Cui, J.; Chou, H.; Shaheen, S. E.; Jabbour, G. E.; Anderson, J.; Lee, P.; Kippelen, B.; Peyghambarian, N.; Armstrong, N. R.; Marks, T. J. *Adv. Mater.* **1999**, *11*, 730.
(5) Zhang, Y.-D.; Hreha, R. D.; Jabbour, G. E.; Kippelen, B.; Peyghambarian, N.; Marder, S. R. *J. Mater. Chem.* **2002**, *12*, 1703.
(6) Li, X.-C.; Yong, T.-M.; Gruener, J.; Holmes, A. B.; Moratti, S. C.; Cacialli, F.; Friend, R. H. *Synth. Met.* **1997**, *84*, 437.
(7) Bellmann, E.; Shaheen, S. E.; Thayumanavan, S.; Barlow, S.; Grubbs, R. H.; Marder, S. R.; Kippelen, B.; Peyghambarian, N. *Chem. Mater.* **1998**, *10*, 1668.
(8) Klärner, G.; Lee, J. I.; Lee, V. Y.; Chan, E.; Chen, J. P.; Nelson, A.; Markiewicz, D.; Siemens, R.; Scott, J. C.; Miller, R. D. *Chem. Mater.* **1999**, *11*, 1800.
(9) Meerholz, K.; Müller, C.-D.; Nuyken, O. In *Organic Light Emitting Devices*; Müllen, K., Scherf, U., Eds.; Wiley VCH: Weinheim, Germany, 2006; Chapter 9, p 293.
(10) Bayerl, M. S.; Braig, T.; Nuyken, O.; Müller, D. C.; Gross, M.; Meerholz, K. *Macromol. Rapid Commun.* **1999**, *20*, 224.
(11) Müller, C. D.; Braig, T.; Nothofer, H.; Arnoldi, M.; Gross, M.; Scherf, U.; Nuyken, O.; Meerholz, K. *Chem. Phys. Chem.* **2000**, *1*, 207.
(12) Crivello, J. V. *J. Polym. Sci., Part A: Polym. Chem.* **1999**, *37*, 4241.
(13) Inoue, S.; Aida, T. *Cyclic Ethers*, In: *Ring-Opening-Polymerisation*; Ivin, K. J., Saegusa, T., Eds.; Elsevier Applied Science Publishers: New York, 1984; Vol. 1, p 185.
(14) Chang, S.-C.; Liu, J.; Bharathan, J.; Yang, Y.; Onohara, J.; Kido, J. *Adv. Mater.* **1999**, *11*, 734.
(15) Carter, J.; Wehrum, A.; Dowling, M. C.; Cacheiro-Martinez, M.; Baynes, N. D. B. *Proc. SPIE—Int. Soc. Opt. Eng.* **2003**, *4800*, 34.
(16) Birnstock, J.; Blassing, J.; Hunze, A.; Scheffel, M.; Stossel, M.; Heuser, K.; Wittmann, G.; Wörle, J.; Winnacker, A. *Appl. Phys. Lett.* **2001**, *78*, 3905.
(17) Bacher, A.; Erdelen, C. H.; Paulus, W.; Ringsdorf, H.; Schmidt, H.-W.; Schuhmacher, P. *Macromolecules* **1999**, *32*, 4551.
(18) Bacher, E.; Jungermann, S.; Rojahn, M.; Wiederhirn, V.; Nuyken, O. *Macromol. Rapid Commun.* **2004**, *25*, 1191.
(19) Domercq, B.; Hreha, R. D.; Zhang, Y.-D.; Larribeau, N.; Haddock, J. N.; Schultz, C.; Marder, S. R.; Kippelen, B. *Chem. Mater.* **2003**, *15*, 1491.
(20) Müller, C. D.; Falcou, A.; Reckefuss, N.; Rojahn, M.; Wiederhirn, V.; Rudati, P.; Frohne, H.; Nuyken, O.; Becker, H.; Meerholz, K. *Nature* **2003**, *421*, 829.
(21) Braig, T.; Müller, D. C.; Gross, M.; Meerholz, K.; Nuyken, O. *Macromol. Rapid Commun.* **2000**, *21*, 583.
(22) Bacher, E.; Bayerl, M.; Rudati, P.; Reckefuss, N.; Müller, C. D.; Meerholz, K.; Nuyken, O. *Macromolecules* **2005**, *38*, 1640.
(23) Hartwig, J. F.; Louie, J. *Tetrahedron Lett.* **1995**, *36*, 3609.
(24) Guram, A. S.; Rennels, R. A.; Buchwald, S. L. *Angew. Chem., Int. Ed.* **1995**, *34*, 1348.
(25) Goodson, F. E.; Hauck, S. I.; Hartwig, J. F. *J. Am. Chem. Soc.* **1999**, *121*, 7527.
(26) Yamamoto, T.; Nishiyama, M.; Koie, Y. *Tetrahedron Lett.* **1998**, *39*, 2367.

MA060844O